



Title	Estimation of nonlinearities from pseudodynamic and dynamic responses of bridge structures using the Delay Vector Variance method
Authors(s)	Jaksic, Vesna, Mandic, Danilo P., Karoumi, Raid, Basu, Biswajit, Pakrashi, Vikram
Publication date	2016-01-01
Publication information	Jaksic, Vesna, Danilo P. Mandic, Raid Karoumi, Biswajit Basu, and Vikram Pakrashi. "Estimation of Nonlinearities from Pseudodynamic and Dynamic Responses of Bridge Structures Using the Delay Vector Variance Method." Elsevier, January 1, 2016. https://doi.org/10.1016/j.physa.2015.08.026 .
Publisher	Elsevier
Item record/more information	http://hdl.handle.net/10197/10435
Publisher's statement	This is the author's version of a work that was accepted for publication in Physica A: Statistical Mechanics and its Applications. Changes resulting from the publishing process, such as peer review, editing, corrections, structural formatting, and other quality control mechanisms may not be reflected in this document. Changes may have been made to this work since it was submitted for publication. A definitive version was subsequently published in Physica A: Statistical Mechanics and its Applications (441, (2016))
Publisher's version (DOI)	10.1016/j.physa.2015.08.026

Downloaded 2025-12-04 23:06:08

The UCD community has made this article openly available. Please share how this access benefits you. Your story matters! (@ucd_oa)



© Some rights reserved. For more information

ESTIMATION OF NONLINEARITIES FROM PSEUDODYNAMIC AND DYNAMIC RESPONSES OF BRIDGE STRUCTURES USING THE DELAY VECTOR VARIANCE METHOD

Vesna Jaksic

*Dynamical Systems and Risk Laboratory, Civil and Environmental Engineering, School of
Engineering, University College Cork, Ireland
v.jaksic@ucc.ie*

Danilo P. Mandic

*Communication and Signal Processing Research Group, Department of Electrical and
Electronic Engineering, Imperial College, London, UK
d.mandic@imperial.ac.uk*

Raid Karoumi

*Civil and Architectural Engineering, The Royal Institute of Technology (KTH) Stockholm,
Sweden
raidk@kth.se*

Bidroha Basu

*Department of Civil Engineering, Indian Institute of Science, Bangalore, Karnataka, India
bidrohabasu@gmail.com
Dynamical Systems and Risk Laboratory, Civil and Environmental Engineering, School of
Engineering, University College Cork, Ireland*

Vikram Pakrashi*

*Dynamical Systems and Risk Laboratory, Civil and Environmental Engineering, School of
Engineering, University College Cork, Ireland
v.pakrashi@ucc.ie*

* Corresponding Author

*Address: Department of Civil and Environmental Engineering, School of Engineering,
University College Cork, Cork, Ireland*

Email: v.pakrashi@ucc.ie

Phone: 00353 857394824

Fax: +353 (0)21 427 6648

Keywords: Delay Vector Variance (DVV), Signal Nonlinearity, System Identification,
Instrumentation, Condition Monitoring, Bridge.

Abstract

Analysis of the variability in the responses of large structural systems and quantification of their linearity or nonlinearity as a potential non-invasive means of structural system assessment from output-only condition remains a challenging problem. In this study, the Delay Vector Variance (DVV) method is used for full scale testing of both pseudo-dynamic and dynamic responses of two bridges, in order to study the degree of nonlinearity of their measured response signals. The DVV detects the presence of determinism and nonlinearity in a time series and is based upon the examination of local predictability of a signal. The pseudo-dynamic data is obtained from a concrete bridge during repair while the dynamic data is obtained from a steel railway bridge traversed by a train. We show that DVV is promising as a marker in establishing the degree to which a change in the signal nonlinearity reflects the change in the real behaviour of a structure. It is also useful in establishing the sensitivity of instruments or sensors deployed to monitor such changes.

1. Introduction

Monitoring of structural responses for the purpose of structural damage detection is widespread [1-4] and such approaches generally depend on the expectation that system responses are related to modal parameters, which are functions of physical properties of the structure [3]. Damages or alterations to a structure can change the dynamic response characteristics and a shift of such characteristics with respect to a benchmark condition can be indicative of structural health [5]. The need for quantitative, global damage detection methods that can be applied to complex structures has led to continued research and development of methods that examine changes in the vibration characteristics of the structure [6, 7]. Quantification of linearity or nonlinearity of the response signals from structural systems and their link to the nature of the structure and changes within is an important

problem which has not yet received significant attention. In other fields, this has been investigated through time series methods employing the outputs of system responses and then attempting to relate a marker of the response to the nonlinearity in the system [8-10].

The importance of addressing structural characteristics under limited, vague, imprecise measurements, or lack of information regarding the structure, or the input has been felt for some time and researchers have approached this problem at different levels employing a range of methods. A structural system has been considered to be a linear filter and chaotic interrogation has been employed to assess nonlinearities [11]. Response dependent white noise has also been used in this regard [12]. In fact, statistical approaches towards characterising or monitoring dynamic responses,, or the utilisation of output-only data [6, 13-17] have now become popular in the context of system identification, damage detection or structural health monitoring. Still, there remains significant information requirement on the structural side that is key to such detection unless a well-established benchmark is created through extensive modelling or experimentation. Works not requiring benchmarking may still be dependent on significant instrumentation and the number of experimentation required may be relatively high [18]. Otherwise, assessment of nonlinearity employing changes in the frequency domain responses is also popular [19-22]. Additionally, addressing identification of properties of structures using wavelet based analysis or other time frequency techniques [23-25] are also present. However, most of these studies have focused on the development of the theoretical methodology and the related experiments are based on scaled models tested under controlled laboratory conditions [26-29]. In this regard, a relatively traditional approach [30-32] towards assessing and interpreting system parameters and estimates of linearity or nonlinearity, requires significant information regarding the system and the input along with controlled experiment is still the main guiding force behind the development and the applications of these methodologies. For larger structures, some work is available in

terms of identification of events or anomalies [33], but output-only assessments of dynamic responses have not yet received significant attention. This can be explained by the fact that full scale testing is relatively difficult to carry out and it is only recently that groups equipped with novel signal processing methodologies are investigating large structural systems. In this regard, the assessment of structural responses of output only condition can be of significant interest, especially in terms of assessing the extent of nonlinearities. The investigation into how the estimates of variability in the response signal of large structural systems relate to the behaviour of the structure can provide insights directly, without assuming the input or the systems model. This model-free approach can be extremely attractive since such approaches can work even better when relevant information regarding the input or the system model is available. Additionally, these methods can be adapted for a wide variety of structures and testing conditions without having to customise it for the particular application.

In this study, the Delay Vector Variance (DVV) method is employed to quantify extent of nonlinearity of the structural system response in order to examine to what extent the nonlinearity of the response signal is linked to changes that the structural system is exposed to. The advantage lies in employing output-only signals from the system without completely knowing the system or the input. The paper demonstrates the ability of DVV to recognise events during rehabilitation or vehicular passage using in-situ structural measurement sensors. Two full-scale experiments on large structures are considered. The first example is an impact damaged prestressed concrete bridge where DVV is applied to analyse the bridge responses, monitored during the rehabilitation works incorporating a network of strain gauges located in and around the damaged region. The works were part of an emergency rehabilitation following the impact of a vehicle passing underneath the bridge [34]. The second example is a single-span composite railway bridge carrying one ballasted truck. The bridge is light and flexible and vibrates easily when a train passes [35]. The first example is

dependent on pseudo-dynamically measured data while the second utilises dynamic time series data. Nonlinearities of the structural responses are estimated and compared for variability of loading in the two structures and the extent to which such nonlinearity estimates can be interpreted and utilised. The work is also a first interdisciplinary investigation of using a method of this nature for assessing such large structures where the model is almost always not available, vague, uncertain or imprecise.

2. Delay Vector Variance (DVV) Methodology

2.1 Background to DVV Method

A popular technique for detecting the nature or nonlinearity of time series is the surrogate data method [36] which was originally motivated by statistical hypothesis testing. The method presents an indirect way of estimating nonlinearity [11]. The DVV method was initially introduced by Mandic and Chambers [37] and was further elaborated and tested in Gautama et al. [38, 39] and Mandic et al. [40]. The method characterises a time series based upon its predictability and compares the results to those obtained for linearised versions of the signal, i.e. surrogate data. This characterisation, although not requiring any prior knowledge about the signal, is robust to the presence of noise, straightforward to interpret and visualise nonlinearity, and typically exhibits improved performance over other available methods [39, 41]. The method has been successfully applied in the past to analyse the nature of biomedical signals [38, 42-44], financial fluctuations [45], mechanical systems [46], and offshore floating structures [47]. Gautama et al. [38] have found that a difference in signal nonlinearity can also be attributed to a difference in system nonlinearity. Application of DVV method in diagnostic medicine showed that the linear or nonlinear nature of the signal may convey information concerning the health condition of the subject [42, 48, 49, 50]. The Root Mean Square (RMS) deviation of the DVV scatter diagram from the bisector line is

considered to be a reasonable quantitative estimate of signal nonlinearity. Jaksic et al. [47] recently investigated the dynamic response signatures of a scaled model tension leg platform for floating wind turbines in an ocean wave basin and found that a change in signal nonlinearity can reflect real time behaviour of the structure along with the sensitivity of the measuring devices.

2.1 DVV Methodology

The method is based on time delay embedding representation of a time series $x(n)$, $n = 1, 2, \dots, N$. The DVV method is extensively explained in Mandic et al. [40] and for a given embedding parameter m , it can be summarised [39, 42, 43], in following steps:

- 1) Reconstruct the phase-space and obtain the set of delay vectors (DVs) in phase space

$$\mathbf{x}(k) = [x_{k-\tau m}, \dots, x_{k-\tau}]^T, \quad k = 1, \dots, N - m + 1 \quad (1)$$

where N denotes the length of time series and τ denotes time lag (delay).

- 2) Compute the mean μ_d and standard deviation σ_d over all pairwise Euclidian distances between DVs [38]

$$d(i, j) = \|x(i) - x(j)\|, \quad (i \neq j) \quad (2)$$

- 3) The sets $\Omega_k(r_d)$ are generated by grouping those DVs that are within a certain Euclidean distance to $\mathbf{x}(k)$ so that

$$\Omega_k(r_d) = \{x(i) \mid \|x(k) - x(i)\| \leq r_d\} \quad (3)$$

i.e. sets that consist of all DVs that lie closer to $\mathbf{x}(k)$ than the certain distance r_d calculated:

$$r_d(n) = \mu_d - n_d \sigma_d + (n - 1) \frac{2n_d \sigma_d}{N_{tv} - 1}; \quad n = 1, \dots, N_{tv} \quad (4)$$

in other words, taken from the interval $[\max\{0, \mu_d - n_d \sigma_d\}; \mu_d + n_d \sigma_d]$, uniformly spaced, where n_d is a parameter controlling the span over which to perform the DVV

analysis, usually set to be 3 and N_{tv} , number of target variance, indicates how fine the standardized distance is uniformly spaced.

- 4) For every set $\Omega_k(r_d)$, the variance of the corresponding targets $\sigma_k^2(r_d)$ is computed.

The average over all sets $\Omega_k(r_d)$ normalised by the variance of the time series, σ_x^2 , yields the measure of unpredictability, ‘target variance’, $\sigma^{*2}(r_d)$:

$$\sigma^{*2}(r_d) = \frac{(1/N) \sum_{k=1}^N \sigma_k^2(r_d)}{\sigma_x^2} \quad (5)$$

Considering a variance measurement valid, too few points for computing a sample variance yields unreliable estimates of the true variance. Jianjun et al. [49] suggest that the set of $\Omega_k(r_d)$ should contain at least $N_0 = 30$ DVs. A sample of 30 data points for estimating mean or variance is the general rule-of-thumb [38, 42, 43].

If two DVs of a predictable signal are close to one another in terms of their Euclidean distance, they should have similar targets. Hence, the presence of strong deterministic component within a signal will result in the smaller target variances for small spans r_d [42, 49]. The minimal target variance $\sigma_{min}^{*2} = \min_{r_d}[\sigma^{*2}(r_d)]$ represents the amount of uncertainty present within the time series and has upper bound which is unity. The reason for this is that all DVs belong to the same set of $\Omega_k(r_d)$ when r_d is sufficiently large. Therefore the variance of the corresponding target of those DVs will be almost equal to that of the original time series. As a result of the standardisation of the distance axes the resulting DVV plots are relatively straightforward to interpret. The resulting DVV curves are plotted with the standardised distance r_d on horizontal axis and normalised variance σ^{*2} on vertical axis. At the extreme right, DVV plots smoothly converge to unity, because for maximum spans, all DVs belong to the same set, and the variance of the targets is equal to the variance of the time series. If this is not the case, the span parameter n_d should be increased [39, 43]. If the

surrogate time series yield DVV plots similar to that of original time series, it indicates that time series is likely to be linear and vice versa [40].

Performing DVV analysis on the original and a number of surrogate time series, a DVV scatter diagram can characterise the linear or nonlinear nature of time series, i.e. if the DVV scatter diagram coincides with the bisector line, then the original time series is adjudged to be linear [39]. Thus, the deviation from the bisector line is an indicator of nonlinearity of the original time series [39, 42]. As the degree of nonlinearity increases, the deviation from bisector line grows too.

The deviation from bisector line can be quantified by the root mean squared error (RMSE) between the σ^{*2} 's of the original time series and the σ^{*2} 's averaged over the DVV plots of the surrogate time series. Thus, a single test statistic t^{DVV} is calculated [43]:

$$t^{DVV} = \sqrt{\left\langle \left(\sigma^{*2}(r_d) - \frac{\sum_{i=1}^{N_s} \sigma_{s,i}^{*2}(r_d)}{N_s} \right)^2 \right\rangle_{\text{valid}_{r_d}}} \quad (6)$$

where $\sigma_{s,i}^{*2}(r_d)$ is the target variance at the span r_d for the i^{th} surrogate, and the average is taken over all spans r_d that are valid in all surrogate and original DVV plots.

2.3 Parameters for DVV Analysis

The time lag is set to unity for convenience, $\tau = 1$, embedding dimension $m = 3$, maximal span parameter $n_d = 3$, the number of standardised distances for which target variances are computed $N_{tv} = 50$, number of surrogates considered $N_s = 25$, and number of reference DVs considered $N_{sub} = 200$ (or 100 where small data sets are available) [38, 39]. The deviation from bisector line of scatter plot quantified by the root mean squared error, will be referred to as RMSE. The authors have carried out prior tests over a number of theoretical and small scale experimental studies to ensure that the parameters values chosen for m and τ elicit

consistent results that converge to the estimated nonlinearity based on a jointly optimised set of values for these parameters corresponding to the true embedding dimension.

3. Analysis on an Impact Damaged Prestressed Bridge

The pseudo-dynamic measurements of a damaged bridge structure during rehabilitation through continuous monitoring is analysed first. By pseudo-dynamic response, it is meant that the sampling of strains is carried out once per minute, but over the period of a few days. The case is interesting as this is an output-only estimate analysing time series which are product of varied natural and human activities imposed on a large structure over a significant period of time. The product of DVV analysis of recorded data and its surrogates, i.e. RMSE, are compared with respect to specific events during the rehabilitation, as well as with the data collection locations. For details regarding this full scale experiment, we refer to [34, 51]. The following sections provide information on the full scale testing based on such literature for completeness.

3.1 Details of Damage

A two-span continuous slab-girder bridge consisting of six precast prestressed U8 type simply supported concrete beams, connected by a continuity diaphragm was damaged by impact force to its soffit (Figure 1). An internal beam was significantly damaged in which the tendons of the beam remained intact but the concrete was crushed from the impact. An unknown redistribution of stresses took place following the impact. . There was no structural cracking in the prestressed concrete beams following the damage in an unloaded state or due to the passage of vehicles. This qualitatively supports the fact that the concrete was within a linear compressive zone. Although it was difficult to estimate the existing stresses within the beam, calculations on extreme hypothetical situations revealed that the beams had significant

windows of operation on the compressive and the tensile side from its unloaded state while remaining within the linear elastic zone for global load displacement characteristics. However, this cannot assess to what extent of nonlinearities are manifest in the bridge when different activities are carried out during the rehabilitation process.

3.2 Instrumentation

Nineteen strain gauges (SG) were installed at five preselected monitoring points (MP) (Figure 2). MPs are strategically chosen so that the interaction of the damaged and undamaged beams, including the behaviour of gauges at, near, and away from the damage can be probed. Gauges were installed at the top and at the bottom of the soffit so that the deformations at these two levels could be observed simultaneously. Three gauges at MP2, the centre of damaged location, were embedded to the tendons. The sampling rate was kept at once per minute min and the data was logged in microstrain units. The low sampling frequency is related to the practical implementation of measurements at large scale [51]. The embedded SG were Geokon vibrating wire embedment gauge model 4200 while the rest of the gauges were Geokon vibrating wire SG model 4000.

3.3 Rehabilitation Process

The rehabilitation was carried out by preloading the bridge to either side of the damaged region in order to release some of the high prestressing compressive force in the soffit of the beam. Preloading consisted of placing 20t bales of concrete blocks either side of the damaged region in three stages (total weight 120t). Hydrodemolition and removal of damaged concrete was carried out next, after which rapid-hardening and high-strength repair material was applied to the damaged region. The repair material was a fibre reinforced spray mortar designed to have a 28 day compressive strength of 70 MPa. The preloads were removed from

the top of the bridge after the repair material hardened and had gained adequate strength. The removal of preload was expected to reintroduce some amount of lost prestress in the repaired zone. Prior to the rehabilitation stage, the structure was exposed mainly to diurnal temperature variation. A similar thermal period was also present after the rehabilitation. Some of the gauges were damaged during the rehabilitation process at different times. Embedded SG (SG11, SG12, and SG13) were directly attached to the tendons before the hydrodemolition process and were zeroed at a later time than the other gauges. The monitoring of repair can be divided into seven periods, as shown in Figure 3.

3.4 DVV Analysis: Results and Discussion

The readings of SGs during rehabilitation period at each observed MP as well as the results of DVV analysis, i.e. DVV plots and DVV scatter plots, of the recorded data during each stage of rehabilitation are presented in Appendix 1, which is provided as a supplementary material with this paper.

3.4.1 Thermal Period

This is the time between the installation of the gauges and the application of load during which fluctuations due to the diurnal cycle can be observed. Tensile forces are induced due to temperature increase in the day leading to a positive increase in strain, while cooler temperatures at night cause compressive action leading to a negative strain change. The results of DVV analysis on strain measured during thermal period are shown in Figure 4. The highest RMSE values are obtained for top strain gauges SG18, SG5, and SG6. The higher nonlinearity of SG18 signal is the result of a series of unusual events, i.e. unexpected peaks within the signal (see Appendix 1). The minimum value of RMSE is 0.159 for the top strain gauges SG9 and SG14. The exception in SG10 and the estimated maximum degree of

nonlinearity with an RMSE value of 0.281 is suspected to be related to a partial damage of the gauge during installation. The dominant trend of the undamaged beams is that the top gauges show the higher nonlinearity of the signal than the corresponding bottom gauges (MP4 and MP5). This is because of the fact that the top gauges were exposed to higher variation in diurnal temperatures, which caused higher variation of strain, than the bottom gauges that were in shadow. The DVV results for the sections of affected beam do not hold this pattern. With exclusion of SG6 and SG7, the degree of the signal nonlinearity is about the same or higher for the bottom strain. This indicates that the redistribution of the strain in damaged region is affected by the existence of the damage.

3.4.2 Preloading Period

The preloading consisted of placing concrete bales staged in three main applications in order to reduce an increase of compressive stress at the soffit. The preloading creates tension in the bottom of the beams, thereby releasing prestressing force, while causing compression at the top of the beam. The preload also introduces a prestrain in and around the damaged zone. At the centre of damage, the embedded gauges are expected to undergo tension and the top gauges compression. SG10 is identified as damaged at this point, although it does react somehow insensitively to events during the bridge rehabilitation. Figure 5 shows the results of DVV analysis of recorded strain for preloading period. The preloading period is very short which resulted in reduced number of reference DVs considered when analysed. Therefore the comparison of results between the repairing stages would not be appropriate unless the lengths of time series are significantly longer. The highest degree of nonlinearity of the signal is recorded by SG16. The reason for this is the sudden jumps in strain data (which are predominantly negative) to positive values of high amplitude created by the tension in the bottom of the beam. A similar phenomena is recorded by SG12 which shows second highest

degree of nonlinearity of data. Around the same period, with little delay, a similar, but smaller jump appears in records of SG1, SG2, and SG3 and does not result in comparably high RMSE. These are probably the periods of load application when the strain redistribution within the concrete was taking place. There is still the same relationship between degrees of nonlinearities in section E-E, that is greater nonlinearity in top SG than in the bottom, although with negligibly reduced RMSE in comparison with the previous stage. All other sections are affected, and the degrees of nonlinearities of top and bottom SGs are reversed or noticeably changed in value. In general, this period exhibits lower degree of nonlinearity than for the thermal period. Pakrashi et al. [51, 52] point out the appearance of bumps in strain data due to the redistribution of stress affecting already fractured concrete. Here, even with the limited number of data for DVV analysis, it seems that the method was capable to detect this change.

3.4.3 Hydrodemolition Period

The recorded strain data are expected to reflect disturbance due to the hydrodemolition activity. Also, it would be anticipated that the gauges along the beam soffit would experience more disturbance as they are located closer to the region of removal. The soffit gauges show a greater disturbance than those at the top of the beams. The sharp jumps or noise in readings can be explained by the nature of the disturbance and for most gauges the disturbance is momentary. However, at the centre of damage it is noted that the embedded gauges (SG11, SG12 and SG13) show little reaction since these gauges are attached to the tendons rather than the concrete, which is suffering the bulk of the disturbance from hydrodemolition. This also highlights the efficiency of the hydrodemolition process as it takes concrete away while affecting the tendons minimally. The degree of nonlinearity of the strain recorded by the embedded gauges is noticeably reduced during this period (Figure 6) which proves the fact

that the gauges are not recording the strain of the concrete but that of the tendons. The highest degree of nonlinearity show strain data of two top gauges (SG5 and SG10) of the damaged section, which supports the fact that the strain readings changed noticeably due to hydrodemolition. The gauge SG18 was damaged in this period and went off the typical scale of the strain gauges which resulted in the high nonlinearity of the recorded signal. In general, RMSE is greater for the soffit than for the top gauges, which is in agreement with observations that the soffit gauges do show greater disturbance than those at the top. However, SG1 and SG2 do not follow this pattern most probably due to the redistribution of the strain between damaged and undamaged beam.

3.4.4 Full Loading Application

This is the period just before the application of the repair material, after completion of hydrodemolition and the application of total loading (120t). During this period there is no significant disturbance in the data. However, the damaged gauge SG18 reading remains off the typical scale of the strain gauges. Also, the readings of SG11, SG13, and SG15 show disturbance in the signal for short periods of time which is due to the load application similar to what is exhibited by SG12 and SG16 during the preloading period. This is yet another example of the high variability of the nonlinearity degree of the strain measured in the damaged region during load application in comparison with other measuring points (Figure 7). The degree of nonlinearity of the strain recorded by the embedded gauges is higher than during hydrodemolition period. This is due to the fact that the embedded gauges undergo significant strain changes over a short period of time during this phase. In general, the soffit strain data show greater nonlinearity than the top data, which is in agreement with the fact that the main role of the preloading is to release prestressing force by creating tension in the bottom of the beams while producing compression at the top of the beam.

3.4.5 Shrinkage Period

The period of application of repair material, shrinkage, and initial hardening with embedment of gauges SG11, SG12, and SG13 is called the shrinkage period. At the centre of damage it is expected that the embedded gauges will be significantly affected by the force due to the shrinkage of the repair material. The embedded gauges show the highest increase in strain due to the tensile force from shrinkage of repair material. The top gauges at MP2 show little change in strain as there is no action occurring at this location other than the secondary action from the repair material shrinkage. In general, the top gauges show little change in strain. The gauges located on the soffit of the beams show an increase in tension due to the shrinkage of the repair material (SG15 recorded an unexpected increase in tension). The results of DVV analysis for shrinkage period are shown in Figure 8. The overall observation is that the strain at the top shows greater nonlinearity degree than the strain measured at the soffit of the beam, with exception of SG14. Also, the strain measured in the damaged section B-B (MP2) shows greater nonlinearity than the strain measured at the other sections at the corresponding locations which is consequence of the increase in tensile force due to shrinkage of concrete. The damaged SG18 and SG19 show the extreme values of RMSE.

3.4.6 Unloading Period

The removal of the 120t loading is done in three stages which are reflected as step changes in strain. The top gauges show a minor decrease in compression over this period. The strain records of gauges along the soffit show decrease of the strain representing a significant reduction in tensile force along the soffit of the beams. This is due to the beams adjusting to an intended compression state typical of a prestressed bridge. The unloading stages are clearly identified in the soffit gauges, e.g the approximate level of change of strain in the

soffit at the location of the centre of damage for each set of removal has been observed to be approximately 20 microstrains. The results of DVV analysis of recorded strain for unloading period are shown in Figure 9. The unloading period is very short which resulted in reduced number of reference DV's considered ($N_{sub} = 100$) when DVV analysed. Therefore the comparison of DVV numerical results between the repairing stages would not be appropriate. Overall RMSE for the top gauges readings decrease for this period and are smaller in comparison with bottom gauges. The similar trend of nonlinearities estimated from DVV is the consequence of the minor changes in compression. However, the degree nonlinearity of soffit strain is noticeably greater than of top strain measured, as the soffit strain decrease due to the introduced compression in this zone.

3.4.7 Further Strength Gain

The further strength gain period covers more than four days of strain gauge readings following the removal of load. Very little evidence is present of shrinkage effects except in the first few hours. From this time on diurnal temperature effects dominate the strain changes, as no other action is occurring on the bridge. There is a strong response to the thermal changes with few exceptions. Two of these poorly responsive gauges (SG5 and SG10) are located as external gauges on the top of the damaged region. The soffit gauges show a strong response to the thermal changes. However, the embedded gauges are within the hardened repair material and are therefore shielded from the temperature effects; consequently, the diurnal variations are not observed. The results of DVV analysis on recorded strain for further strength gain period are shown in Figure 10. The observed period is the longest during which the strain measured obtained stable readings. Overall RMSE for the top and bottom gauges readings are very close, with few exceptions. The exceptions of embedded SG12, which have measurements that show more linear behaviour than measurements of the other

gauges since it is sheltered, thus not affected by diurnal temperature variation. The RMSE for the measurements recorded by SG18 and SG19 reflects the malfunctioning of the strain gauges.

3.4.8 Correlation of Top Gauges

Figure 11a shows the variation of RMSE for top gauges. The malfunctioning of the SG10 and SG18 is reflected in DVV results of the recorded signal which are noticeably different in value of the mainstream results obtained for the other gauges. Further, the results of DVV analysis can be used to detect the extreme disturbance in the material. For example, the largest deviation in the DVV results ($\Delta\text{RMSE} = 0.168$) is recorded during the hydrodemolition period with the maximum nonlinearity in strain experienced by the strain gauge at centre of damage (SG5). Moreover, DVV results reflected the disturbances of the small scale experienced by material, such as during the secondary action of shrinkage period when the deviation in the results between top gauges is $\Delta\text{RMSE} = 0.130$. Finally, DVV results on top strain measured during the last stage are approximately the same, gravitating to $\text{RMSE}_{\text{avg}} = 0.168$, which proves that there is no more shrinkage of the concrete, but just diurnal temperature effects resulting in negligible deviation between results ($\Delta\text{RMSE} = 0.015$). In this stage the redistribution of the strain between the beams is established and strain gauges readings is stabilized.

3.4.9 Correlation of Soffit Gauges

Figure 11b shows the variation of RMSE for soffit gauges. Similar to the observation of damaged top gauges, the DVV results reflect the damage of SG19 ever since full load application period. Complimentary to the top SG findings, DVV results of bottom SG reflect the disturbances in the strain recorded by the soffit gauges during the hydrodemolition period

However, the embedded SG record show that the difference in the degree of nonlinearity of recorded signal is $\Delta RMSE = 0.092$. The results confirm the success of the hydrodemolition process since the embedded gauges attached to the tendons were not affected by the hydrodemolition process, thus resulting in low RMSE in comparison to the rest of the soffit gauges attached to concrete. Further, DVV results of soffit gauges show the change of strain due to the high tension and section adjustment to the loading during the preload and full loading application. For all other stages, i.e. thermal, shrinkage, unloading, and full strength gain period, the difference in the soffit strain nonlinearity is small. This is the evidence that the readings of the SG are stable.

3.4.10 Comparisons of the Beams

In order to test performance of DVV analysis on pseudo-dynamic data the relationships between the damaged beam and the undamaged beams on either side is analysed. Figure 12 shows a plot comparing the RMSE of three beams for each repairing stage. ‘Beam 3’ is the damaged beam while ‘Beam 2’ and ‘Beam 4’ are undamaged beams (see Figure 2), represented by SG5, SG1, and SG18, respectively. The bridge is expected to be within the linear zone of response with good relationships between the beams. From Figure 12a, it is evident that ‘Beam 2’ and ‘Beam 3’ strains are of the same nonlinearity pattern. During the preloading period the compression is increased at the top in order to reduce the tension at the soffit and as the consequence, the degree of the nonlinearity computed from strain response of damaged beam is proportionally higher during the some stages (hydrodemolition, full loading and shrinkage period), while it is almost the same for other stages of repair (unloading and further strength gain period). This is in agreement with the expected behaviour during the bridge repair, as the curing of concrete is finished and strain distribution

between the beams is established more stable reading is obtained resulting in almost the same degree of nonlinearity.

The DVV results for ‘Beam 4’, represented by SG18, reflect the malfunctioning of this strain gauge detected during the hydrodemolition period (Figure 12 b and 12c). However, it appears that DVV results of the SG18 are in good agreement with SG5 during the first three stages of repair (Figure 12b). There are two possible reasons for this. The first reason could be the fact that the SG18 readings went off the scale, but still appeared ‘regular’ from the point of view that such large readings were still magnified and scaled based on the changes in different stages of work, so that DVV was not affected by the change of the amplitude of the signal but was governed by the shape of the signal. The second reason, could be related to the short observation period, i.e. limited number of data for DVV analysis available during this period. Otherwise, the disagreement in RMSE pattern of SG18 with SG5 and SG1 is an indicator of malfunctioning.

4 Scaling property

4.1. Background on scaling property

A time series is expected to exhibit scaling/multi A scaling behaviour if the underlying system governing the time series has distinguishable features/information at different temporal scale. As the complexity and hence the nonlinearity of a system increases, the system is expected to exhibit multi-scaling behaviour. With increase in multi-scaling, the degree of nonlinearity is expected to be higher.

In the previous section, the change in degree of nonlinearity was described using RMSE calculated by taking difference between the DVV obtained from the original time series and

that obtained from the surrogates generated based on the original time series. By construction, the surrogates are linearised version of the original time series. Hence, if the original time series is linear in nature, the RMSE value is expected to be low, whereas higher value of RMSE might indicate high degree of nonlinearity present in the original time series. However, higher RMSE might not always indicate high degree of nonlinearity, as in situations where the statistical properties of DVVs of original and surrogate time series are significantly different, RMSE can become high. In situations where original time series is linear, the difference between the DVVs of original and surrogate time series can be reasonably expected not to show high multi-scaling behaviour, even though in some situations the RMSE can be high. Hence, an alternative multi-scaling based analysis has been performed on the difference series obtained from the DVV of the original time series and the DVV obtained from the averages of all the surrogate time series. The basic methodology to estimate multi-scaling properties of a time series is given below.

Consider a time series $x(t)$, $t = v, 2v, \dots, kv, \dots, T$ where v is the time resolution and T is the time for which data is available. To characterize the statistical evolution of the time series $x(t)$, the Hurst exponent corresponding to q -th order moment can be estimated as follows:

- 1) Estimate q -th order moment of increments of $x(t)$ as,

$$K_q(\tau) = E[|x(t + \tau) - x(t)|^q] / E[|x(t)|^q] \quad (7)$$

where time interval τ can vary between v and τ_{max} . In the present study, τ_{max} has been considered to be 19, as suggested in literature [53, 54].

- 2) Estimate the generalized Hurst exponent $H(q)$ from the scaling relation:

$$K_q(\tau) \sim \left(\frac{\tau}{v}\right)^{qH(q)} \quad (8)$$

If the value of generalized Hurst exponent does not vary with q , then the series $x(t)$ is considered to exhibit chiefly mono-fractal behavior and the generalized Hurst exponent coincides with the Hurst exponent, whereas if generalized Hurst exponent varies considerably

then the series is said to be multi-fractal and different exponent characterize the scaling of different moments of the time series.

4.2. Scaling property results

To investigate effectiveness of multi-scaling in quantifying degree of nonlinearity, strain data from damaged prestressed bridge had been analysed. Strain data obtained from each of the strain-gauge for seven stages of repair were first analysed to estimate DVV. Following this, 25 linearised surrogate series for each SG for each repair stage were generated and the average of all those surrogates was estimated. DVV obtained from the original and DVV estimated from the average of generated surrogates series were then obtained as a time series. Following this, generalized Hurst exponent corresponding to each of the differenced DVV time series were calculated using the procedure explained above. The generalized Hurst exponent $H(q)$ for several moments q along with the RMSE were then noted for each of the time series. A few typical plots of $qH(q)$ versus moment q for some of the strain gauges were plotted in Figure 13, for brevity.

During unloading period (stage 6) SG1 shows multi-scaling which corroborates with high RMSE value corresponding to that stage. On the other hand, when the RMSE is low, the Hurst exponent shows simple-scaling for SG1. For SG8 the Hurst exponent indicates simple-scaling for every stage and the RMSE were found to be low for all the stages. For embedded SG13, the RMSE was found to be high for unloading and strength gain periods (stages 6 and 7), and multi-scaling has been observed. Those observations indicated that for undamaged locations, we observe multi-scaling when the RMSE value is high and simple-scaling when RMSE is low, meaning that Hurst exponent and RMSE results are consistent. For SG10, the RMSE is found to be high for unloading period (stage 6) and low for the remaining stages. However, it can be observed that unloading period exhibits simple-scaling and only

preloading and hydrodemolition periods (stage 2 and 3) shows multi-scaling behaviour, even though the RMSE is low corresponding to those two stages. For SG18, RMSE is high for shrinkage and unloading periods (stages 5 and 6), but multi-scaling is observed for thermal and hydrodemolition periods (stages 1 and 3), and there is a slight deviation from simple-scaling corresponding to stages 5 and 6. On the other hand, for SG19, the RMSE is high for hydrodemolition and strength gain periods (stages 3 and 7) and low for the remaining stages, but the figure shows multi-scaling behaviour for every stage except thermal and full loading periods (stage 1 and 4). Overall, the results indicated that for damaged locations RMSE and Hurst exponent does not show always similar behaviour. In some cases we obtained low (high) RMSE and simple-(multi-)scaling, but there are situations where we obtain simple-scaling even though RMSE is high and vice-versa. This indicated that, for undamaged locations RMSE is sufficient to model degrees of nonlinearity, but for damaged locations, RMSE along with scaling/multi-scaling properties is necessary to examine nonlinearity of the system.

Further, damaged beams exhibit multi-scaling behavior mainly during the preloading and hydrodemolition period, and slightly multi-scaling behaviour has been observed during thermal and unloading periods, whereas for full loading, shrinkage and strength gain periods we obtained a simple scaling behaviour. Results using the thermal period in the beginning is indicative of a situation where only thermal affect is observed and hence there will be some degree of complexity associated to this stage. During preloading and hydro demolition complex stress redistribution takes place and it was expected to obtain high multi-scaling behaviour during those two stages. During repair and hardening of repair material, the processes are expected to be stable and not much complexity in terms of stress redistribution was supposed to be present. Preload removal introduced some degree of complexity in the stress pattern and that was reflected in the generalized Hurst exponent. In the last stage, the

concrete gained further strength and the only complexity is due to thermal affect, which is expected to be nominal. The conclusions drawn from generalized Hurst exponent obtained from the difference between surrogates and the real signal corresponds to the physical understanding of the phenomena corresponding to the seven stages of bridge repair and is observed to be a potential tool to augment and complement the capability of DVV.

5 Analysis on a Single Span Steel-Concrete Composite Bridge

The DVV method was implemented next on a large bridge with responses measured at a significantly higher time resolution where the dynamics of the structure form the governing signature of the structural responses. The dynamic response of a composite bridge structure traversed by trains with continuous monitoring employing different sensors is considered in the second example. The time series corresponding to responses to train loadings on a large bridge structure over a period of time are used in the study. The outcome of DVV analysis of recorded data and its surrogates, i.e. RMSE, are compared with respect to the type of the train crossing and location of dynamic measurements.

The experimental site and *in situ* measurements are part of research conducted by Division of Structural Design and Bridges, Department of Civil and Architectural Engineering, KTH, Stockholm. The following sections describing the bridge, monitoring instrumentation, and the details of the trains used in the experiment are based on relevant literature [35, 55-57] are included here for completeness.

5.1 Description of the Bridge

Skidträsk Bridge, located in the North of Sweden, is a simply supported single span steel-concrete composite bridge caring a single ballasted track and spanning 36m. The rails are supported by concrete sleepers on a layer of ballast underneath which is a layer of sub-ballast.

The ballast layers are on a reinforced concrete slab, which transfers the load from the tracks to two steel beams. The width of the concrete slab is 6.7m and it varies in height between 30 and 40 cm. The steel beams also have a variable cross section. The cross section of the bridge is shown in Figure 15.

5.1.1 Material and Structural Properties of the Bridge

The material properties for the observed bridge are summarised in Table1 and include information on the steel, concrete, ballast, and the concrete and ballast combined (concrete deck with the ballast). In the case of the combined section of concrete and ballast, the stiffness is not altered but the mass is increased. The damping of such structure is small (0.5% - 1.5%) and consequently, the effects of this low damping do not become significant for the structure vibrating under the passage of train in terms of dynamic responses.

5.1.2 Traffic Loading on the Bridge

The bridge is used by freight and passenger trains, details of which are given in the Table 2. The Swedish Steel Arrow train, a common iron ore freight train in Sweden, is a particularly frequent loading on the bridge. The Steel Arrow (SA) usually comprises 2 power cars or locomotives and 26 wagons (388m total length).

The trains listed in Table2 can be generally divided in two groups according to their characteristics; group A (Train 1, 2, 4, and 9) and group B (Train 3, 5, 6, 7, and 8). There are two different characteristics among the train model of group A; maximum acceleration and maximal speed. On the other hand group B trains have more differences among themselves (i.e. the number of locomotives and wagons, the maximal acceleration and speed, the number of bogies, and loading). A special case is Train 7 with just few common characteristics with group B trains.

5.1.3 Instrumentation

Permanent and temporary monitoring systems are installed consisting of 6 and 10 sensors, respectively (Figure 15). The permanent system consisted of 4 strain gauges situated on the east beam, at midpoint and quarter-point, on the top and the bottom flanges (CH1 to CH4), 3 Si-flex SF1500S accelerometers for vertical deck accelerations were installed: two of them are on the east beam at midpoint and quarter-point (CH5 and CH7); and the third, on the west beam at midpoint (CH6), 2 strain transducers (B-WIM sensors) on the concrete slab at midpoint and quarter-point (CH9 & CH11), to measure transversal strain, and A temperature gauge (CH8). The temporary system consisted of four accelerometers installed around the mid-span of the bridge (midpoint of the central sleeper (T-1), end point of the central sleeper (T-2), in the rail placed at the level of the central sleeper (T-3), and in the ballast between two sleepers (T-4)). The signals from the two optical laser sensors allowed the determination of the number of wagons of the train and the distance between two axles, and this then allowed the calculation of train speed and the determination of train type by the distance between axles, bogies and wagons. The distance between the two optical sensors was 26.05 meters. During the first day, the sampling rate was 150 Hz and a Bessel (anti-aliasing) filter was applied with a filter cut-off frequency of 20 Hz. During the rest of the year in which the system was in use, the sampling rate was increased to 600 Hz and the filter cut-off frequency of the anti-aliasing filter to 75 Hz [35, 57].

5.1.4 Measurements and Data Filtering

The list of the instruments locations is given in Table 3. The examples of strain and acceleration responses to train passage are shown in Figure16 and 17 for beams and slab, respectively. The recorded bridge responses to all train types crossing are shown in Appendix

2 along with related DVV analyses results. There are two stages in filtering data. In the first stage only the responses of the bridge due to passage of the train are included, i.e. the acceleration of the bridge recorded prior to the train passage and after the bridge reaches its equilibrium position (saturation of vibration) is excluded (Figure 18). In the second stage the data that went off the scale for no apparent reason are excluded. These data are categorised as bad data. The duration of the periods of bad data are very small (sporadic single points), but their contribution in the signal nonlinearity analysis can be significant.

5.2 Results of DVV Analysis

The DVV analysis results of the acceleration and strain recorded in bridge due to train traffic loading are shown in Appendix 2, while the parameters chosen for DVV analysis are given in Section 2.3.

5.2.1 Strain Measured in the Beams

The results of DVV analysis of the strain measured in the east beam at top (TF) and bottom (BF) flange at the mid and quarter span for all trains are shown in Figure 19. The nonlinearity of TF strain is prominently greater than that of BF in all cases observed. Hence the DVV method can distinguish the location of the measurement in respect to the type of the loading, i.e. TF that is in compression has higher and BF that is in tension has lower RMSE. Moreover, Figure 19 shows the difference in RMSE between measurements obtained at the midspan and quarter span regardless of the strain gauge location in relation to the cross-section, i.e. top or bottom. Hence, it is possible to relate the magnitude of the response and the location of the measurement. The RMSE calculated at midspan is generally greater than for the quarter span, which is expected as the magnitude of deformation is greater at midspan. This is more prominent for the bottom flange measurement than that of the top flange

measurement since the deformation of the top flange are constrained with the concrete slab. This reflects the fact that the difference in degree of nonlinearity of TF measurements between mid- and quarter-span is small for each train model observed. For all cases observed, the RMSE for TF ranges from 0.340 to 0.407 and 0.333 to 0.402, for mid and quarter span, respectively. This shows that there is no obvious correlation between the train characteristics and degree of nonlinearity of TF. However, there is the decreasing trend in strain nonlinearity observed for group A trains and unloaded train of group B (Train 3) with the maximum RMSE at the TF midspan and minimum at BF quarter span.

Regard the BF, for the trains of group A the nonlinearity of the strain at the midspan is greater than at quarter span, which is in agreement with findings for top flange. However, the trend between RMSE of strain measured at the mid- and quarter-span of the BF of the loaded group B trains (Trains 5, 6, 7, and 8) show that the linearity is greater for the signal measured at the quarter span than at the midspan. This could be due to the fact that as the vehicle leaves the bridge its speed increases and the redistribution of the strain take place. The reason for this could be the characteristics of the train. The obvious possibility is that this phenomenon is driven by the loadings, where trains of group A and unloaded train of group B hold the same trend of DVV results. The other possibility is that the choice of DVV parameters is such that DVV scatter plot is crossing the bisector line (see Appendix 2) giving lower RMSE values for quarter span BF of group B trains. Even with this adjustment of DVV parameters, the relationship between degree of nonlinearity of strain at bottom flange and train characteristics is hard to establish. A part of the presence of this nonlinearity can be explained from the friction at the bearing locations, which is usually difficult to assume or estimate beforehand even in theoretical modelling of the structure before detailed inspection and testing are carried out suspecting such behaviour.

5.2.2 Acceleration of the Beams

The results of DVV analysis of beam acceleration are shown in Figure 20. The RMSE values suggest larger nonlinearity at mid span and smaller nonlinearity at quarter-span, for the responses of the bridge to the crossing of Group A train with the exception of the Train 4. This train passage also produces accelerations with the visibly highest nonlinearity. This is likely to be linked to the fact that it has lower speed, 61.2km/hr, than the other trains from this group. The same pattern, as majority of group A train, hold Train 3 of group B, which is unloaded train. Hence, these results support the theory that the existence of the loading could be detected by the DVV analysis of the strain and acceleration measurements. The nonlinearity degree is about the same (approximately 0.2) for the Trains 5, 6, and 7 (group B trains) for three measurement locations. The visibly highest nonlinearity of the acceleration measured is recorded for Train 8, between 0.371 and 0.39. This train belongs to the group B train category, but moves with the lowest speed. The conclusion that could be driven from here is that the train passes over the bridge with the lower speed the acceleration nonlinearity will increase. In that case, the increase in the signal nonlinearity will also depend on the type of train in such that the train with the wagons (wagon loading) will produce the beam acceleration response signal of the greatest nonlinearity.

5.2.3 Strain of Concrete Slab

Figure 21 shows the results of DVV analysis for the strain measured in the slab at mid- and quarter-span. The degree of nonlinearity of strain at these two locations is about the same for the train crossing. For the crossing of the group A trains the degree of nonlinearity is high ranging from 0.350 to 0.450 with exception of Train 4 that has visibly lower linearity, which appears to be linked to the train low crossing speed in comparison to the rest in the group. In general, the results of DVV analysis of the concrete slab strain for the train group A crossing,

the nonlinearity increases with the increase of train speed. The RMSE obtained for the group B train crossing the bridge has the same relationship to the speed of train. However, the level of nonlinearity is visibly lower, with range from 0.201 to 0.253. This is the proof that the train speed is not the only contributor to the nonlinearity. The observation and comparison of the train characteristics leads to conclusion that the loading of the train or/and number of the wagons are the factors that can reduce the nonlinearity of slab transversal strain. Also, the RMSE for the bridge response to the unloaded Train 7 with no wagons is higher than for Train 3 or 5, yet these three trains have the same speed. Further the degrees of nonlinearity in transverse slab strain negligibly decrease with the load when two trains of same characteristic compared (Train 3 and 5). These observations also highlight the challenges in relation to monitoring large dynamic systems from output-only conditions.

6 Conclusions

The Delay Vector Variance (DVV) method has been employed to characterise the behaviour of two bridges through analysis of their response and the estimation of nonlinearities in their pseudo-dynamic and dynamic responses. For a pseudo-dynamic analysis of the rehabilitation of the prestressed concrete bridge, analysing each stage of repair and comparing the results obtained from different measurement suggests that the variability in estimated nonlinearity is observed to be representative of the various anthropogenic activities carried out on the structure and the relationship of various components are also found. The malfunctioning instruments (e.g. strain gauges) can also be detected to a certain extent using this method. Upon analysis of the damaged and undamaged beams, the processing of the original strain data has been observed to be beneficial for indicating both sudden and gradual changes. The analysis of the DVV results obtained from the single span composite bridge dynamic data has showed that the degree of nonlinearity of the bridge response does not depend only on bridge

structural characteristics but on the vehicle crossing, i.e. on the interaction between the two, especially when the system nonlinearity is related to the friction at the bearings, which has a direct effect on the nonlinearity related to live loading. The link between the speed of the vehicle and degree of nonlinearity of slab transversal strain is established, where if speed increases the nonlinearity increases for the bridge considered. The other influential factor for the degree of nonlinearity of the slab strain response is the weight of the moving vehicle.

It is difficult to compare the two observed systems from the structural point of view presented in this paper. It is even harder to compare the responses of these two systems. However the pseudo-dynamic data analysed after the repairs reveal that the degree of nonlinearity of the strain measured becomes stable (approx. 0.166), while DVV plots indicate linear behaviour of the bridge response. For dynamic loading of the composite bridge the degree of nonlinearity varies between locations and responses measured. It is generally higher for the same types of measurements and this high nonlinearity is reflected in DVV plots.

The DVV method in combination with online structural monitoring can be used for fast and inexpensive structure assessment. The initial values of RMSE should be calculated for ambient vibration of unloaded structure and vibration due to expected loading on the structure. These values should be used as benchmark. Additionally the evolution of the estimated nonlinearities of different components over time may serve as an output-only marker for the assessment of the structural health. Overall, the method is observed to be practical for fast assessment of the health of complex structures through analysis of their real-time responses and this aspect is attractive for the diagnostics of structural health.

Acknowledgements:

Funding statement: The support of the Irish Research Council (known as the Irish Research Council for Science, Engineering and Technology at the time of initiation of funding) Embark Scholarship R13570 is gratefully acknowledged.

The support of Science Foundation Ireland, International Strategic Cooperation Award (ISCA), Ireland–India ISCA Programme, grant no. 12/ISCA/2493 is also acknowledged along with India Study Centre, University College Cork, Ireland.

The authors gratefully acknowledge the involvement and help of the following:

The National Roads Authority, Maudlins, Naas, Kildare, Ireland

South Dublin County Council, Tallaght, Dublin, Ireland

Joe Kelly, Roughan & O'Donovan Consulting Engineers, Dublin, Ireland

Reference

1. Ghaffar, A.M.A. and R.H. Scanlan, *Ambient Vibration Studies of Golden Gate Bridge: I. Suspended Structure*. Journal of Engineering Mechanics 1985. **111**(4): p. 483.
2. Abdel-Ghaffar, A.M. and R.H. Scanlan, *Ambient Vibration Studies of Golden Gate Bridge: II. Pier Tower Structure*. Journal of Engineering Mechanics, 1985. **111**(4): p. 483-500.
3. Doebling, S.W., C.R. Farrar, M.B. Prime, and D.W. Shevitz, *Damage Identification and Health Monitoring of Structural and Mechanical Systems from Changes in Their Vibration Characteristics: A Literature Review*, N. LABORATORY, Alamos, and f.t.U.S.D.o.E. . Editors. 1996, Los Alamos National Laboratory is operated by the University of California for the United States Department of Energy under contract W-7405-ENG-36. p. 136.
4. Gentile, C. and N. Gallino, *Ambient vibration testing and structural evaluation of an historic suspension footbridge*. Advances in Engineering Software, 2008. **39**(4): p. 356-366.
5. Clough, R.W. and J. Penzien, *Dynamics of Structures*. third edition ed, ed. B.J. Clark. 1993, Singapore: McGraw-Hill Book Co.
6. Sohn, H., C.R. Farrar, N.F. Hunter, and K. Worden, *Structural Health Monitoring using Statistical Pattern Recognition Techniques*. ASME Journal of Dynamic Systems, Measurement and Control 2001. **123**(4): p. 706-717.
7. Pakrashi, V., B. Basu, and A. O'Connor, *Nondetection, False Alarm, and Calibration Insensitivity in Kurtosis- and Pseudofractal-Based Singularity Detection*. Journal of Aerospace Engineering, 2009. **22**(4): p. 466-470.

8. Bian, C. and X. Ning, *Evaluating age-related loss of nonlinearity degree in short-term heartbeat series by optimum modeling dimension*. Physica A: Statistical Mechanics and its Applications, 2004. **337**(1–2): p. 149-156.
9. Tsonis, A.A., F.L. Heller, and P.A. Tsonis, *Probing the linearity and nonlinearity in DNA sequences*. Physica A: Statistical Mechanics and its Applications, 2002. **312**(3–4): p. 458-468.
10. Su, Z.-Y., T. Wu, P.-H. Yang, and Y.-T. Wang, *Dynamic analysis of heartbeat rate signals of epileptics using multidimensional phase space reconstruction approach*. Physica A: Statistical Mechanics and its Applications, 2008. **387**(10): p. 2293-2305.
11. Theiler, J., S. Eubank, A. Longtin, B. Galdrikian, and J. Doyne Farmer, *Testing for nonlinearity in time series: the method of surrogate data*. Physica D: Nonlinear Phenomena, 1992. **58**(1–4): p. 77-94.
12. Rüdinger, F. and S. Krenk, *Identification of Nonlinear Oscillator with Parametric White Noise Excitation*. Nonlinear Dynamics, 2004. **36**(2-4): p. 379-403.
13. Sohn, H., J. Czarnecki, and C. Farrar, *Structural Health Monitoring Using Statistical Process Control*. Journal of Structural Engineering, 2000. **126**(11): p. 1356-1363.
14. Parloo, E., S. Vanlanduit, P. Guillaume, and P. Verboven, *Increased reliability of reference-based damage identification techniques by using output-only data*. Journal of Sound and Vibration, 2004. **270**(4–5): p. 813-832.
15. Nagarajaiah, S. and B. Basu, *Output only modal identification and structural damage detection using time frequency & wavelet techniques*. Earthquake Engineering and Engineering Vibration, 2009. **8**(4): p. 583-605.
16. Tibaduiza, D.A., M.A. Torres-Arredondo, L.E. Mujica, J. Rodellar, and C.P. Fritzen, *A study of two unsupervised data driven statistical methodologies for detecting and classifying damages in structural health monitoring*. Mechanical Systems and Signal Processing, 2013. **41**(1–2): p. 467-484.
17. Rizos, D.D., S.D. Fassois, Z.P. Marioli-Riga, and A.N. Karanika, *Vibration-based skin damage statistical detection and restoration assessment in a stiffened aircraft panel*. Mechanical Systems and Signal Processing, 2008. **22**(2): p. 315-337.
18. Pakrashi, V., B. Basu, and A.O. Connor, *A Statistical Measure for Wavelet Based Singularity Detection*. Journal of Vibration and Acoustics, 2009. **131**(4): p. 041015 (6 pages)
19. Peng, Z.K., Z.Q. Lang, S.A. Billings, and Y. Lu, *Analysis of bilinear oscillators under harmonic loading using nonlinear output frequency response functions*. International Journal of Mechanical Sciences, 2007. **49**(2007): p. 1213–1225.
20. Josefsson, A., M. Magnevall, K. Ahlin, and G. Broman, *Spatial location identification of structural nonlinearities from random data*. Mechanical Systems and Signal Processing, 2012. **27**(0): p. 410-418.
21. Jaksic, V. and V. Pakrashi, *Robust Skewness-Kurtosis Descriptor for Damping Calibration from Frequency Response*. Journal of Aerospace Engineering, 2013. **26**(4): p. 887-893.
22. Carrella, A. and D.J. Ewins, *Identifying and quantifying structural nonlinearities in engineering applications from measured frequency response functions*. Mechanical Systems and Signal Processing, 2011. **25**(3): p. 1011-1027.
23. Moyo, P. and J.M.W. Brownjohn, *Detection of Anomalous Structural Behaviours using Wavelet Analysis*. Mechanical Systems and Signal Processing 2002. **16**(2-3): p. 429-445.
24. Pai, P.F. and A.N. Palazotto, *Detection and identification of nonlinearities by amplitude and frequency modulation analysis*. Mechanical Systems and Signal Processing, 2008. **22**(5): p. 1107-1132.

25. Pakrashi, V., B. Basu, and A. O' Connor, *Structural damage detection and calibration using a wavelet-kurtosis technique*. Engineering Structures, 2007. **29**(9): p. 2097-2108
26. Zhang, E., J. Antoni, R. Pintelon, and J. Schoukens, *Fast detection of system nonlinearity using nonstationary signals*. Mechanical Systems and Signal Processing, 2010. **24**(7): p. 2065-2075.
27. Aykan, M. and H. Nevzat Özgüven, *Parametric identification of nonlinearity in structural systems using describing function inversion*. Mechanical Systems and Signal Processing, 2013. **40**(1): p. 356-376.
28. Nichols, J.M., S.T. Trickey, M. Seaver, and S.R. Motley, *Using ROC curves to assess the efficacy of several detectors of damage-induced nonlinearities in a bolted composite structure*. Mechanical Systems and Signal Processing, 2008. **22**(7): p. 1610-1622.
29. Hot, A., G. Kerschen, E. Foltête, and S. Cogan, *Detection and quantification of non-linear structural behavior using principal component analysis*. Mechanical Systems and Signal Processing, 2012. **26**(0): p. 104-116.
30. Masri, S.F., T.K. Caughey, R.K. Miller, and A.F. Saud, *Identification of Nonlinear Vibrating Structures: Part I—Formulation*. Journal of Applied Mechanics, 1987. **54**(4): p. 918-922.
31. Masri, S.F., T.K. Caughey, R.K. Miller, and A.F. Saud, *Identification of Nonlinear Vibrating Structures: Part II—Applications*. Journal of Applied Mechanics, 1987. **54**(4): p. 923-929.
32. Masri, S.F., A.G. Chassiakos, and T.K. Caughey, *Structure-unknown non-linear dynamic systems: identification through neural networks*. Smart Materials and Structures, 1992. **1**(1): p. 45.
33. Omenzetter, P B.J.M. William, and M. Pilate, *Identification of Unusual Events in Multi-Channel Bridge Monitoring Data*. Mechanical Systems and Signal Processing 2004. **18**(2): p. 409-430.
34. Pakrashi, V., J. Harkin, J. Kelly, A. Farrell, and S. Nanukuttan, *Monitoring and repair of an impact damaged prestressed bridge*. Proceedings of the ICE - Bridge Engineering, 2012. **166**(1): p. 16-29.
35. Lorieux, L., *Analysis of train-induced vibrations on a single-span composite bridge*, in *Department of Civil and Architectural Engineering, Division of Structural Design and Bridges*. 2008, Royal Institute of Technology (KTH): Stockholm, Sweden.
36. Schreiber, T. and A. Schmitz, *Surrogate time series*. Physica D: Nonlinear Phenomena, 2000. **142**(3-4): p. 346-382.
37. Mandic, D.P. and J.A. Chambers, *Recurrent Neural Networks for Prediction: Learning Algorithms, Architectures and Stability*, ed. S. Haykin. 2001: John Wiley & Sons, Ltd.
38. Gautama, T., D.P. Mandic, and M.M.V. Hulle, *Signal Nonlinearity in fMRI: A Comparison Between BOLD and MION*. IEEE Transactions on Medical Imaging, 2003. **22**(5): p. 636 - 644.
39. Gautama, T., D.P. Mandic, and M.M.V. Hulle, *The delay vector variance method for detecting determinism and nonlinearity in time series*. Physica D: Nonlinear Phenomena, 2004. **190**(3-4): p. 167-176.
40. Mandic, D.P., M. Chen, T. Gautama, M.M. Van Hulle, and A. Constantinides, *On the characterization of the deterministic/stochastic and linear/nonlinear nature of time series*. Proceedings of the Royal Society A: Mathematical, Physical and Engineering Science, 2008. **464**(2093): p. 1141-1160.

41. Hou, S., Y. Li, and S. Zhao, *Detecting the Nonlinearity in Time Series from Continuous Dynamic Systems based on Delay Vector Variance Method*. International Journal of Engineering and Applied Sciences, 2007. **3**(5): p. 258-263.
42. Gautama, T., M.M.V. Hulle, and D.P. Mandic, *On the characterisation of the deterministic/stochastic and linear/nonlinear nature of time series*, in *DPM-04-05*. 2004, Imperial College London. p. 30.
43. Gautama, T., D.P. Mandic, and M.M.V. Hulle, *Indications of nonlinear structures in brain electrical activity*. Physical Review E, 2003. **67**(4): p. 046204 (5).
44. Kuntamalla, S. and R.G.L. Reddy, *The Effect of Aging on Nonlinearity and Stochastic Nature of Heart Rate Variability Signal Computed using Delay Vector Variance Method*. International Journal of Computer Applications 2011. **14**(5): p. 40-44.
45. Peter Martey Addo, M. Billo, and D. Guegan, *Understanding Exchange Rates Dynamics*. 2013: Documents de Travail du Centre d'Economie de la Sorbonne, Paris, France.
46. Hongying, H. and Y. Fuliang. *Diesel Engine Fault Information Acquisition Based on Delay Vector Variance Method*. in *Knowledge Acquisition and Modeling, 2009. KAM '09. Second International Symposium on*. 2009.
47. Jaksic, V., R. O'Shea, P. Cahill, J. Murphy, D.P. Mandic, and V. Pakrashi, *Dynamic response signatures of a scaled model platform for floating wind turbines in an ocean wave basin*. Phil. Trans. R. Soc. A, 2015. **373**: 20140078(2035).
48. Schreiber, T., *Interdisciplinary Application of Nonlinear Time Series Methods*. Physics Reports, 1999. **308**: p. 1-64.
49. Jianjun, Y., W. Haijun, X. Chunming, W. Yiqin, L. Fufeng, G. Rui, and M. Tiancai. *Nonlinear Analysis in TCM Acoustic Diagnosis Using Delay Vector Variance*. in *Bioinformatics and Biomedical Engineering, 2008. ICBBE 2008. The 2nd International Conference on*. 2008.
50. Andrzejak, R.G., K. Lehnertz, F. Mormann, C. Rieke, P. David, and C.E. Elger, *Indications of nonlinear deterministic and finite-dimensional structures in time series of brain electrical activity: dependence on recording region and brain state*. Physical Review E, 2001. **64**: p. (6 Pt 1):061907.
51. Pakrashi, V., J. Kelly, J. Harkin, and A. Farrell, *Hurst exponent footprints from activities on a large structural system*. Physica A: Statistical Mechanics and its Applications, 2013. **392**(8): p. 1803-1817.
52. Pakrashi, V., J. Harkin, J. Kelly, A. Farrell, and S. Nanukuttan, *Monitoring and repair of an impact damaged prestressed bridge*. ICE - Bridge Engineering, 2012. **166**(Issue BE1): p. 16-29.
53. Di Matteo, T., T. Aste, and M.M. Dacorogna, *Scaling behaviors in differently developed markets*. Physica A: Statistical Mechanics and its Applications, 2003. **324**(1): p. 183-188.
54. Di Matteo, T., T. Aste, and M.M. Dacorogna, *Long-term memories of developed and emerging markets: Using the scaling analysis to characterize their stage of development*. Journal of Banking & Finance, 2005. **29**(4): p. 827-851.
55. Tang, D., *Dynamic response of a composite railway bridge to passing train: Comparison of FEM simulations and measurements*, in *Division of Structural Engineering and Bridges, Department of Civil and Architectural Engineering*. 2012, Royal Institute of Technology (KTH): Stockholm, Sweden 2012.
56. Ülker-Kaustell, M. and R. Karoumi, *Application of the continuous wavelet transform on the free vibrations of a steel-concrete composite railway bridge*. Engineering Structures, 2011. **33**(3): p. 911-919.

57. Martino, D., *Train-Bridge Interaction on Freight Railway Lines*, in *Department of Civil and Architectural Engineering, Division of Structural Design and Bridges*. 2011, KTH (Royal Institute of Technology): Stockholm, Sweden.

LIST OF TABLES

Table 1 Material properties of the bridge [35]

Table 2 Train Characteristics

Table 3 The list of measurements and their locations used in DVV analysis

Table 1

Material	Young's Modulus (GPa)	Poisson's Ratio ν	Density ρ (kg/m ³)
Concrete	32	0.2	2500
Steel	210	0.3	7850
Ballast	-	-	2000
Concrete with additional mass of Ballast	32	0.2	5700

Table 2

Train		1	2	3	4	5	6	7	8	9
No. Locomotives		2	2	2	2	3	2	2	2	2
No. Wagons		0	0	36	0	36	28	0	27	0
Loaded				No		Yes	Yes		Yes	
Max. acc.	(m/s ²)	-0.65	1.22	2.3	-0.42	2.4	-3.4	5	-1.3	1.6
Max. speed	(m/s)	23	50	33	17	33	27	33	18	42
	(km/hr)	82.8	180	118.8	61.2	118.8	97.2	118.8	64.8	151.2
No.Bogies		4	4	76	4	78	60	4	58	4
Distance bogie-locomotive	(m)	20	20	7.7	20	7.7	7.7	7.7	7.7	20
Distance bogie-wagon	(m)	0	0	8.6	0	8.6	8.6	0	8.6	0
Distance loco-bogie	(m)	6.5	6.5	6.28	6.5	6.28	6.28	6.28	6.28	6.5
Distance wagon-bogie	(m)	0	0	5.38	0	5.38	5.38	0	5.38	0
Distance loc & wag bogie	(m)	0	0	5.83	0	5.83	5.83	0	5.83	0
Distance axles (loco)	(m)			2.7		2.7	2.7	2.7	2.7	
Distance axles (wag)	(m)			1.8		1.8	1.8	1.8	1.8	
Locomotive length	(m)			10.4		10.4	10.4		10.4	
Wagon length	(m)	0		10.4		10.4	10.4		10.4	
Load on bogie (loco)	(N/axle)					1.95E+05	1.95E+05		1.95E+05	
	(N/bogie)	9.00E+05	9.00E+05	1.00E+06	9.00E+05	3.90E+05	3.90E+05	3.90E+05	3.90E+05	9.00E+05
Load on bogie (wagon)	(N/axle)					2.25E+05	2.25E+05		2.25E+05	
	(N/bogie)					4.50E+05	4.50E+05		4.50E+05	

Table 3

	STRAIN				ACCELERATION			TRANSVERSAL STRAIN	
Measurement Point	CH1	CH2	CH3	CH4	CH5	CH6	CH7	CH9	CH11
Location	East beam L/2		East beam L/4		East beam L/2	West beam L/2	East beam L/4	Slab L/2	Slab L/4
	Top flange	Bottom flange	Top flange	Bottom flange	Top flange				

LIST OF FIGURES

Figure 1. Damaged region of outer beam (left) and inner beam (right) [34].

Figure 2. Arrangement of multichannel strain gauge network [34].

Figure 3. Strain data from continuous monitoring for two representative strain gauges on the soffit of the bridge (SG3 on undamaged and SG7 on damaged beam), with activities and time zones related to such activities identified.

Figure 4. DVV analysis results of strain gauges measurements obtained during thermal period.

Figure 5. DVV analysis results of strain gauges measurements obtained during preloading period.

Figure 6. DVV analysis results of strain gauges measurements obtained during hydrodemolition period.

Figure 7. DVV analysis results of strain gauges measurements obtained during full load application period.

Figure 8. DVV analysis results of strain gauges measurements obtained during shrinkage period.

Figure 9. DVV analysis results of strain gauges measurements obtained during unloading period.

Figure 10. DVV analysis results of strain gauges measurements obtained during further strength period.

Figure 11. Variation of DVV analysis results on strain measured by a) top and b) bottom strain gauges.

Figure 12. Comparisons of DVV analysis of damaged and undamaged beams.

Figure 13. q vs $qH(q)$ plots for strain gauges 1, 8, 10, 13, 18 and 19. SG stands for strain gauge.

Figure 14. Photograph of Skidträsk Bridge [35].

Figure 15. a) Section of the bridge, b) part of the track at midspan, and c) schematic representation of the bridge span with location of the sensors (accelerometers in red and strain gauges in green).

Figure 16. Strain of the east beam measured at top and bottom flange at the mid- and quarter-span for the Train 2.

Figure 17. Acceleration measured at the top flange of the east and west beam for the Train 2 (dotted line rectangle indicates the region of valid data for DVV analysis).

Figure 18. Transversal strain measured at mid- and quarter-span of the slab for the Train 2.

Figure 19. DVV analysis results of strain gauges measurements for East beam.

Figure 20. DVV analysis results of accelerometer measurements for East and West beam.

Figure 21. DVV analysis results of strain transducers measurements for concrete slab.



Figure1

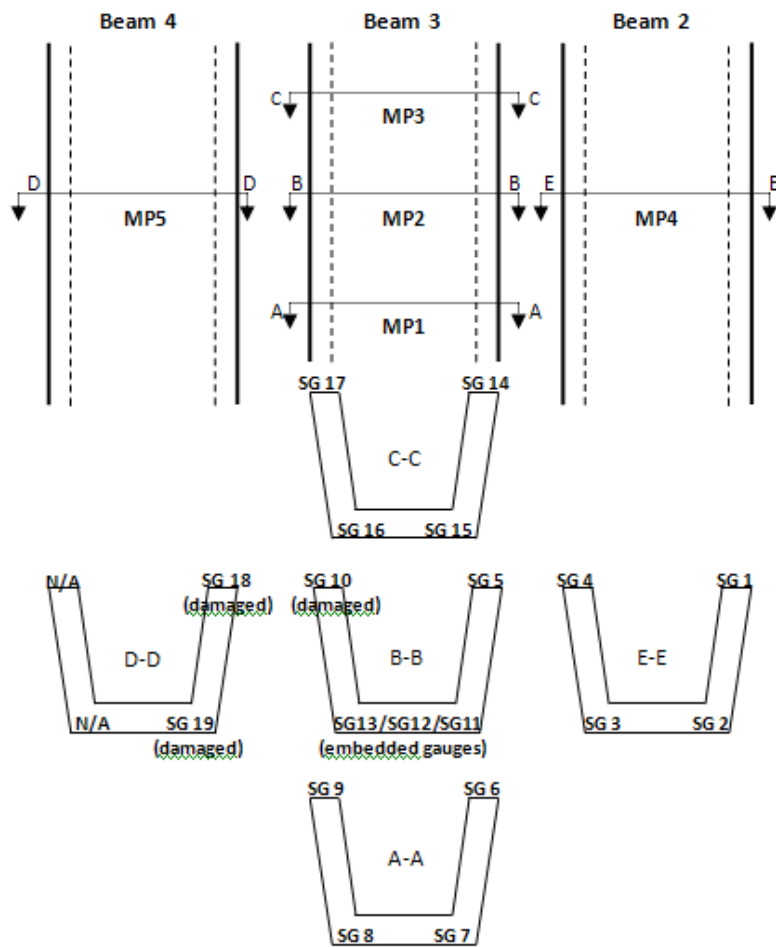


Figure2

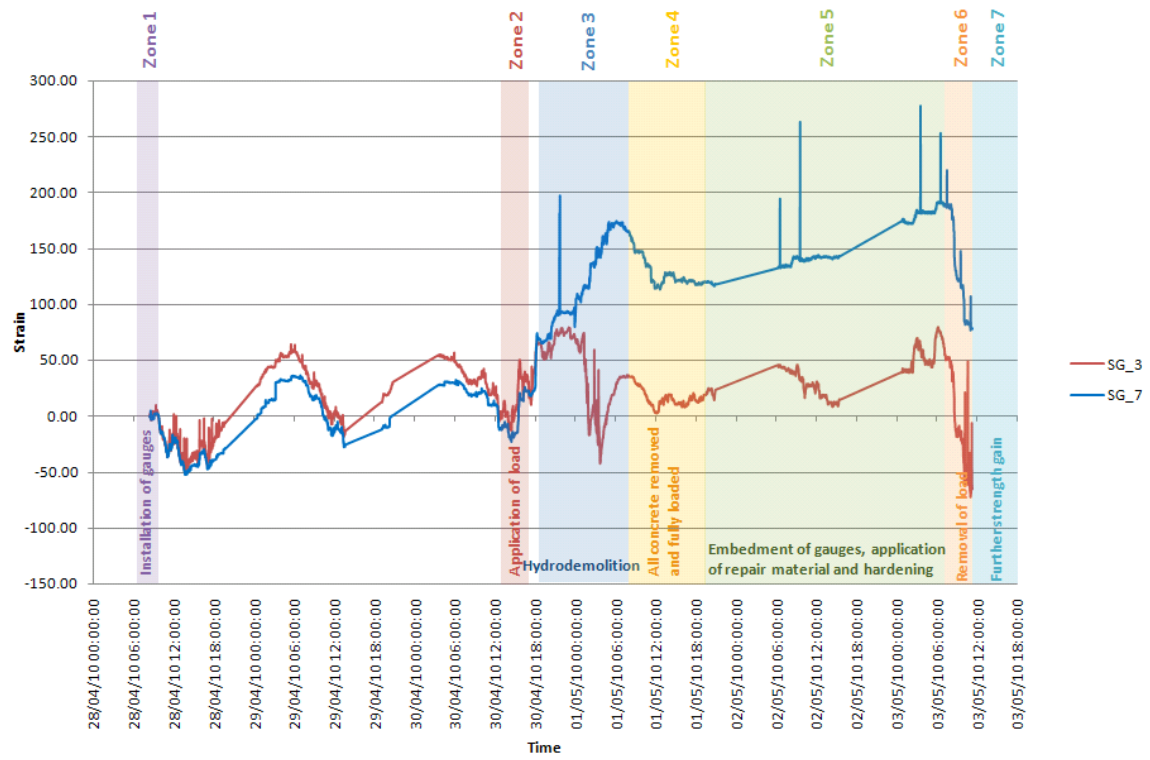


Figure3

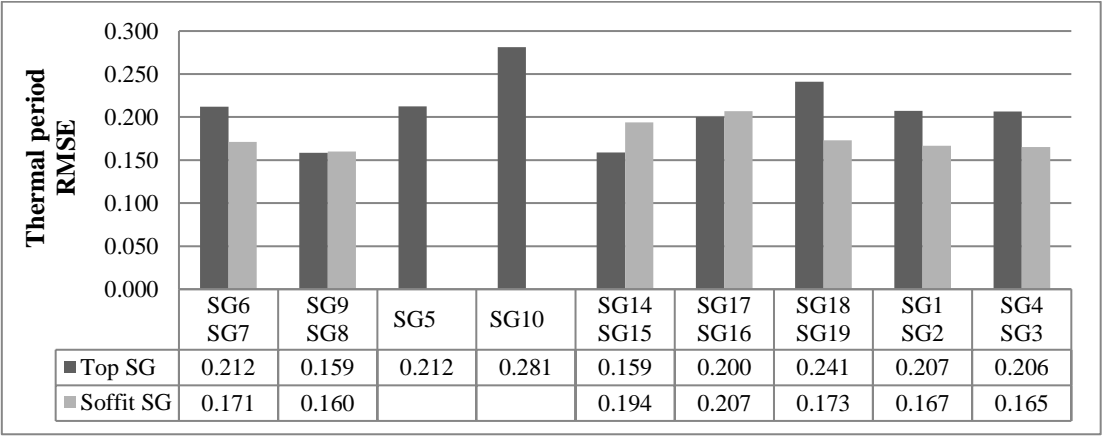


Figure4

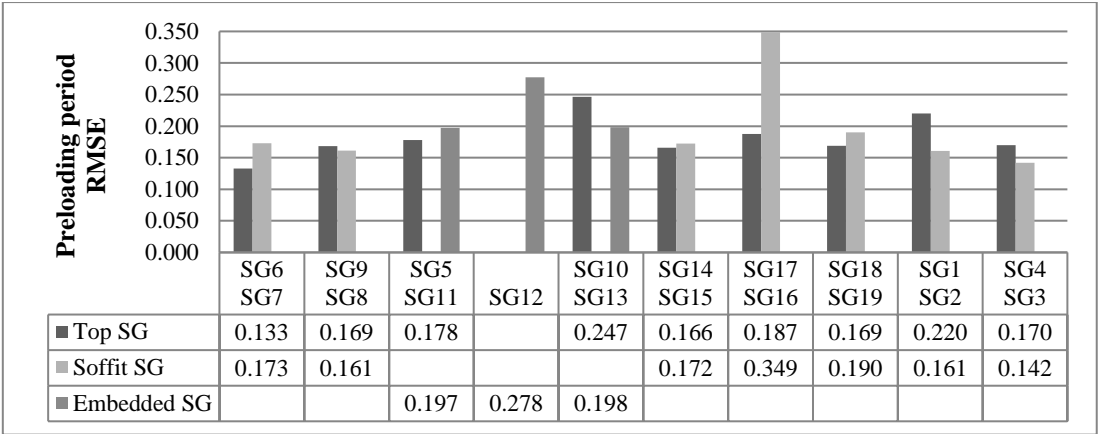


Figure5

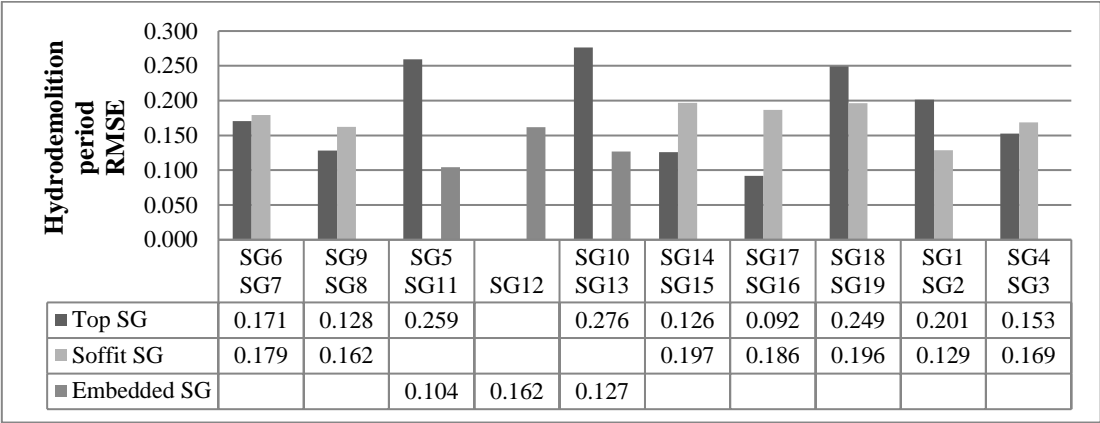


Figure6

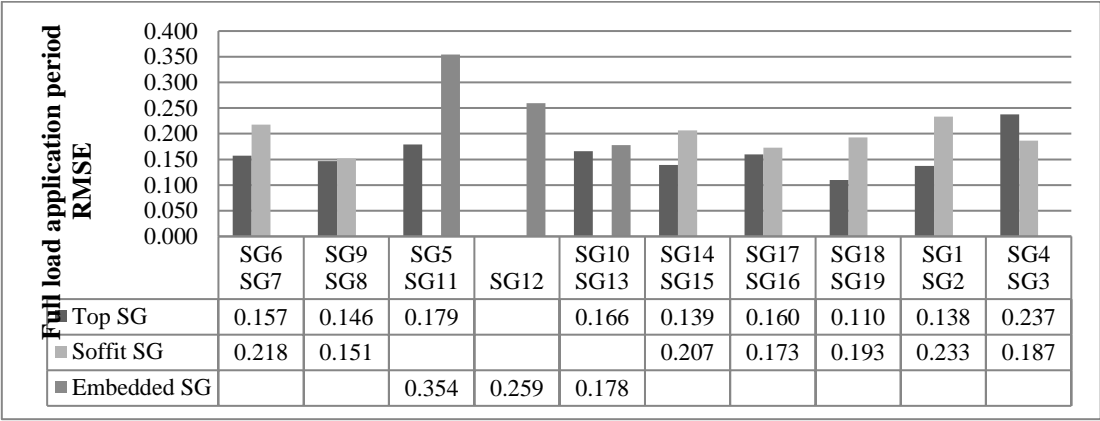


Figure7

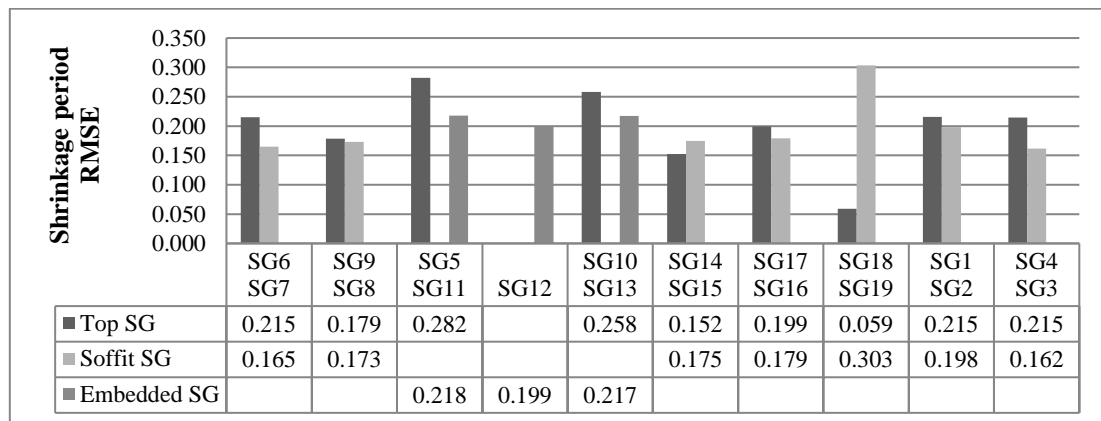


Figure8

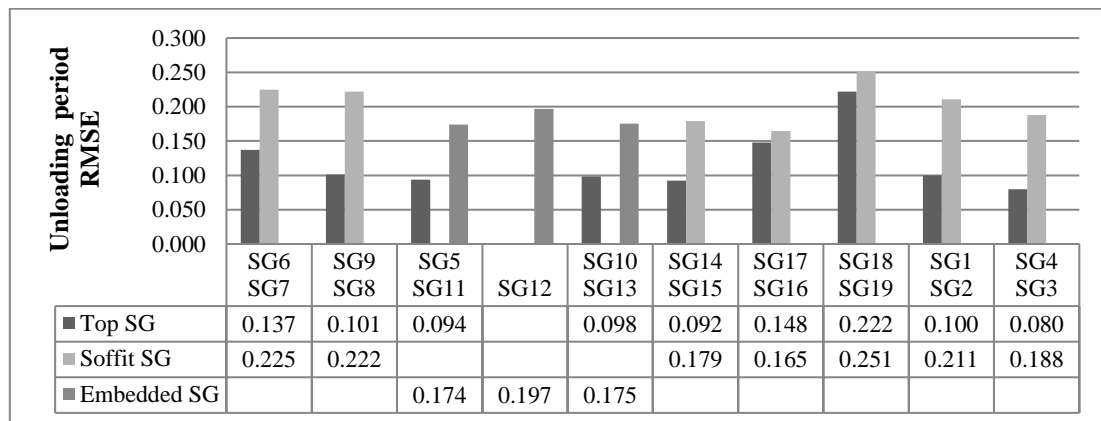


Figure9

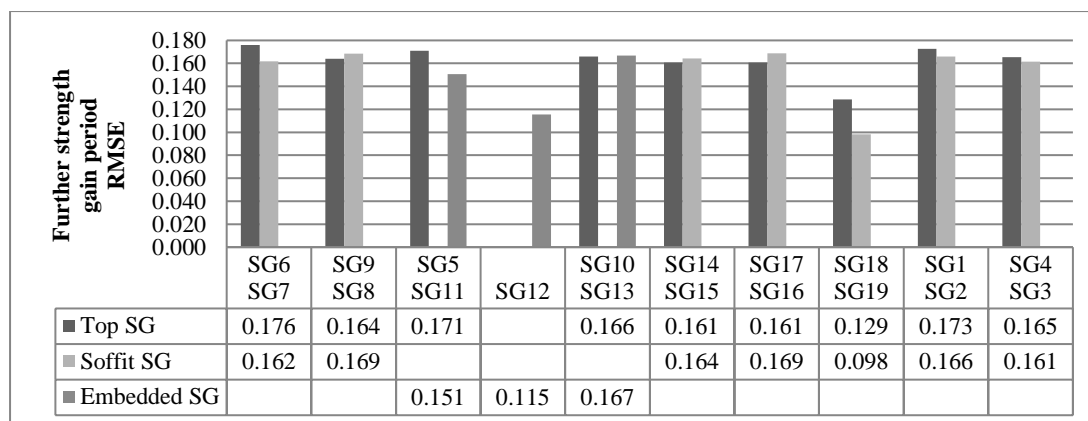


Figure10

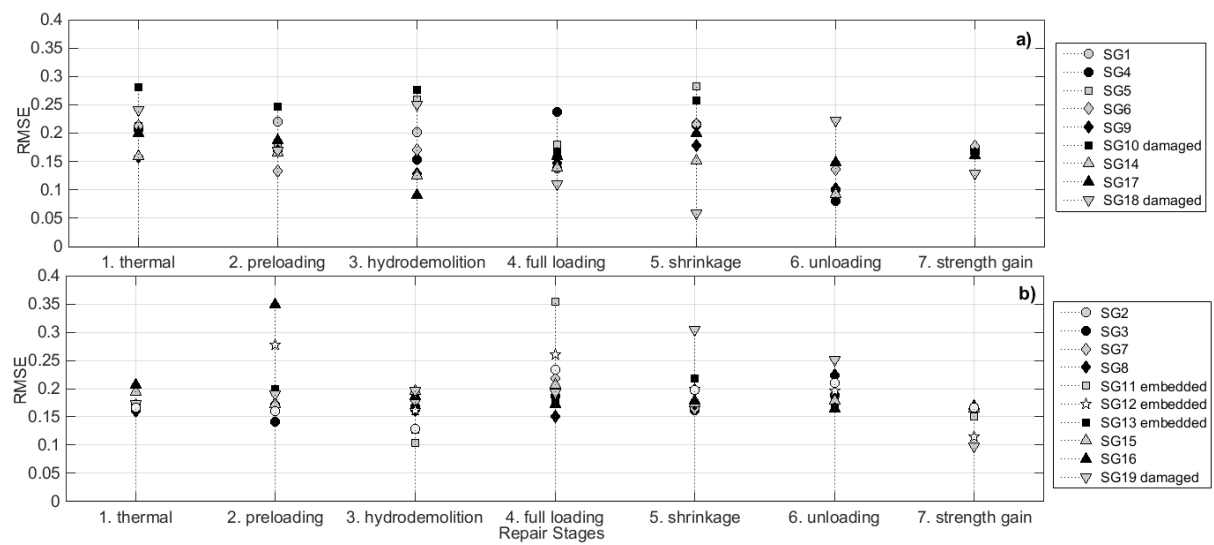


Figure11

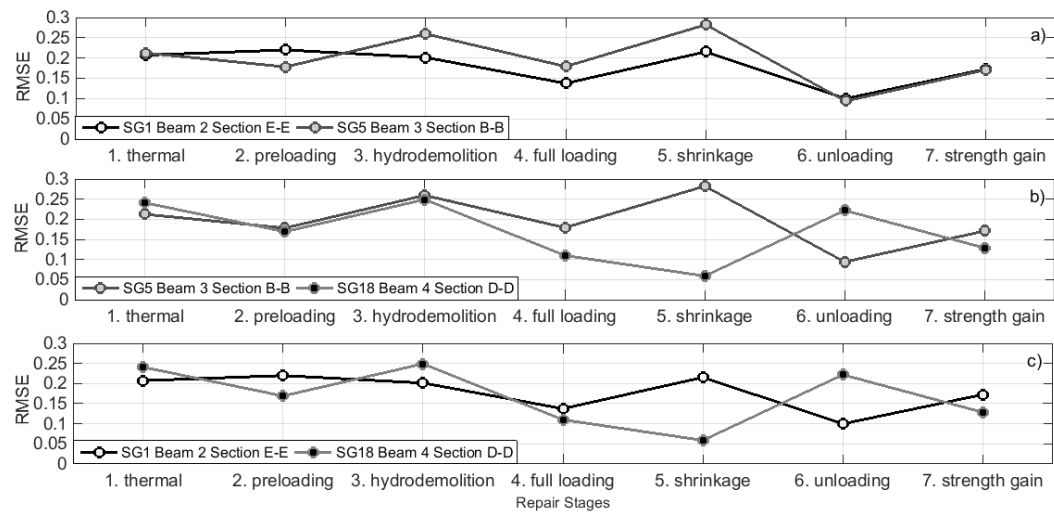


Figure12

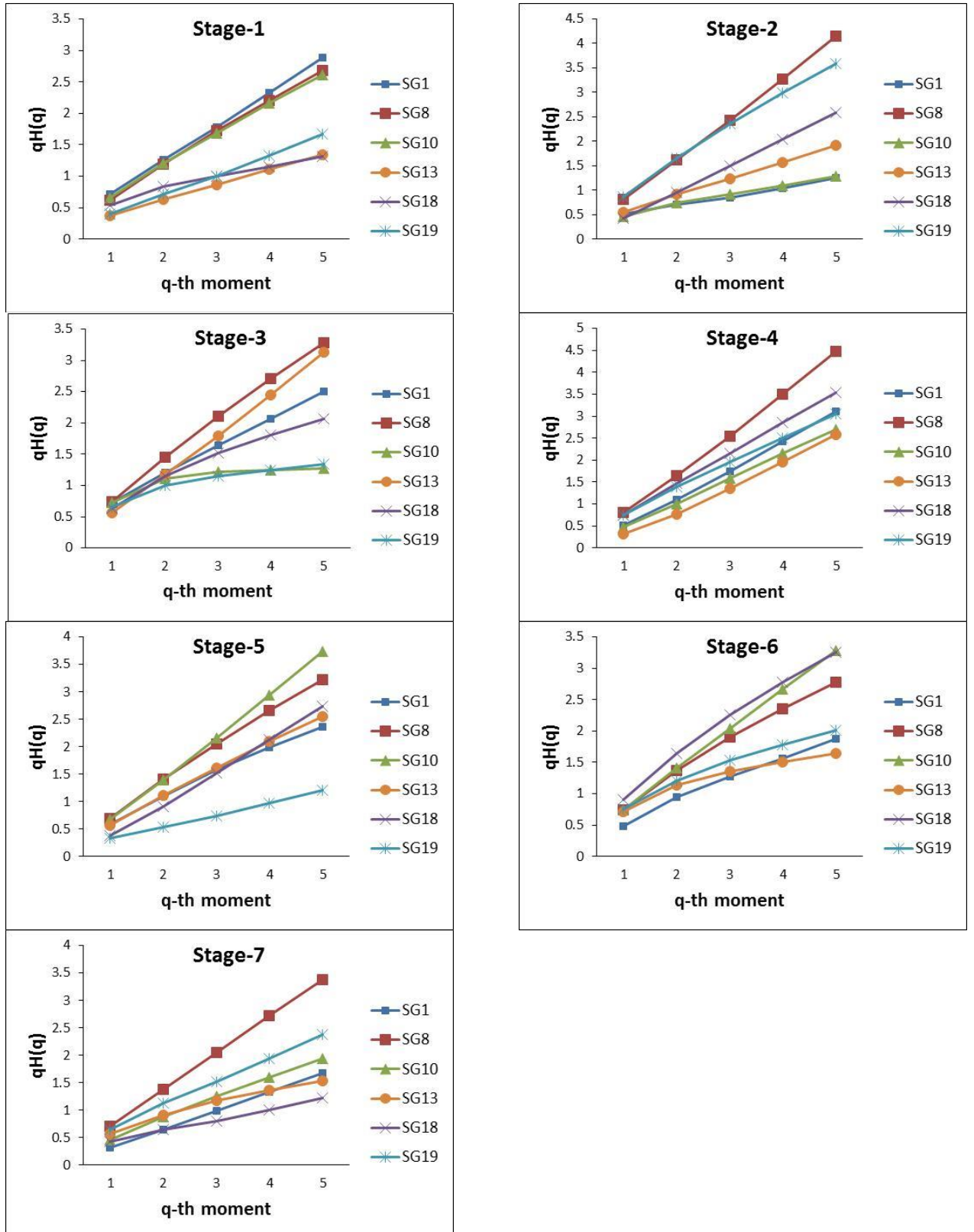


Figure13



Figure14

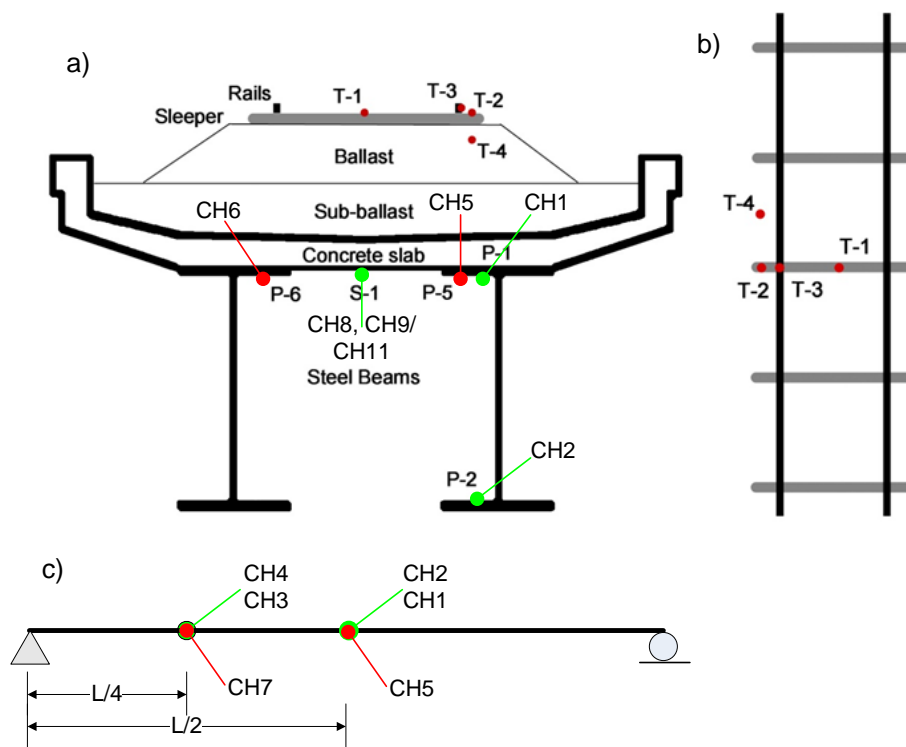


Figure15

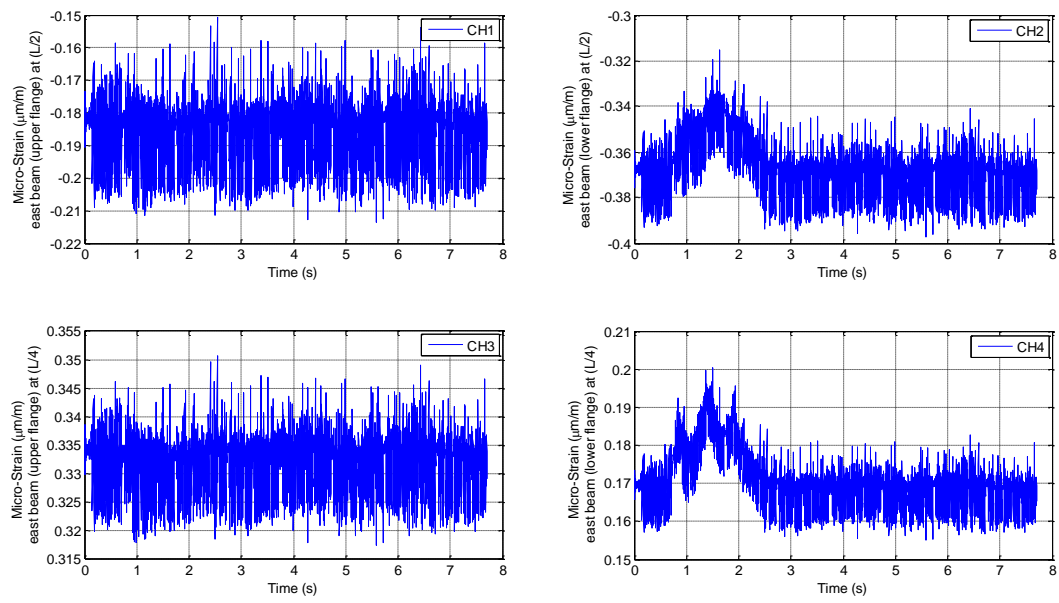


Figure16

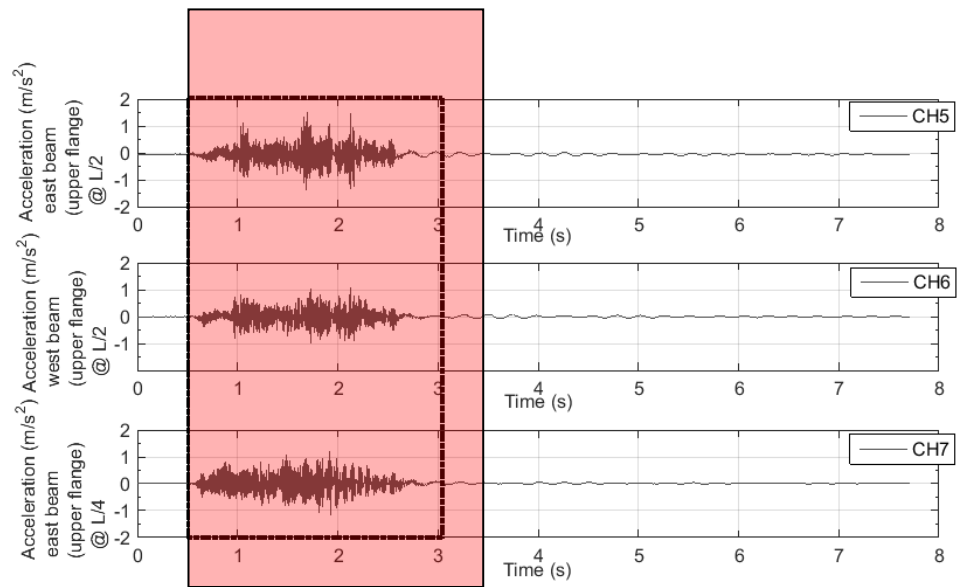


Figure17

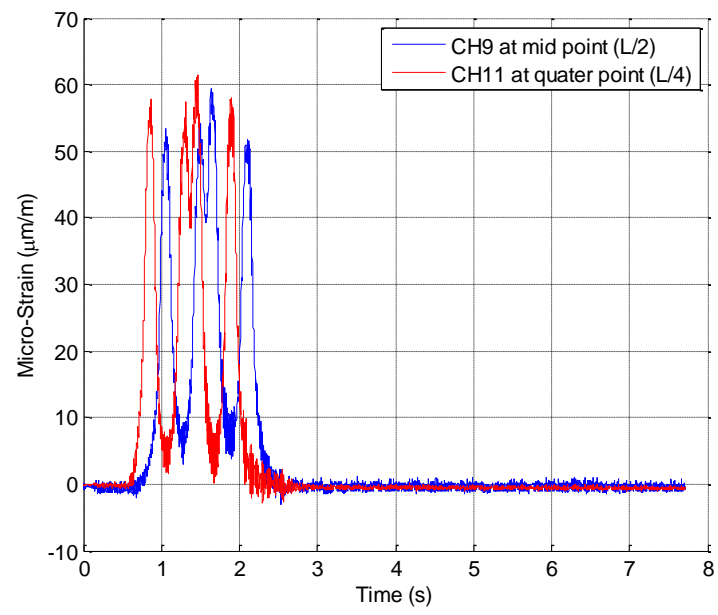


Figure18

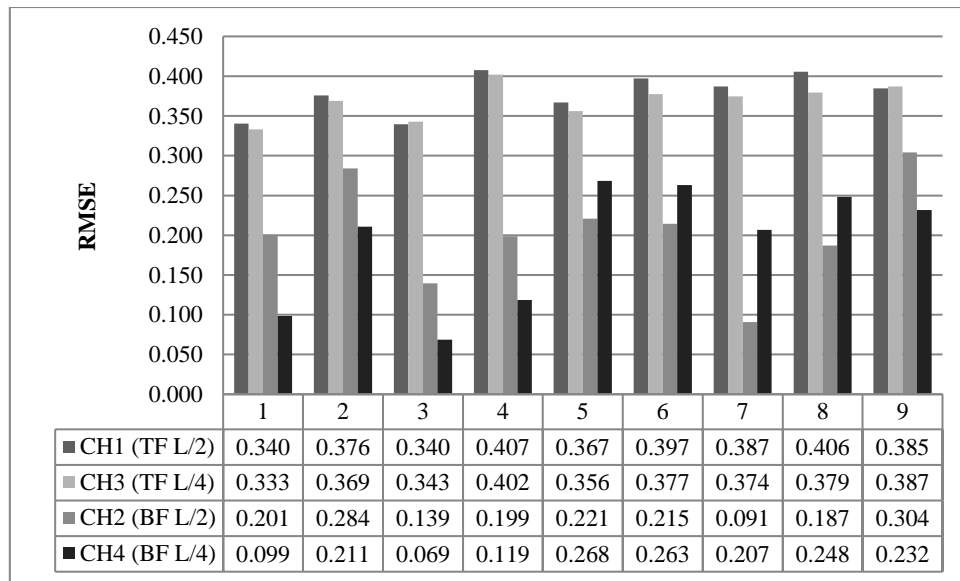


Figure19

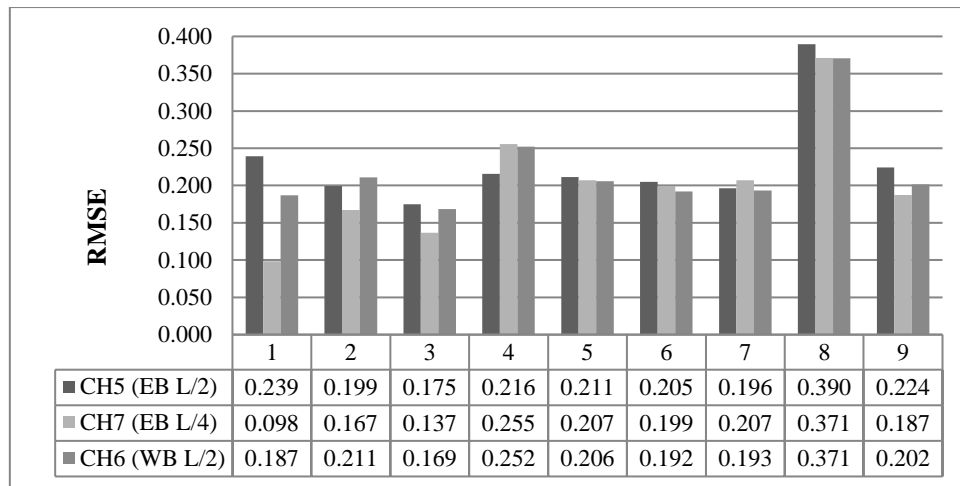


Figure20

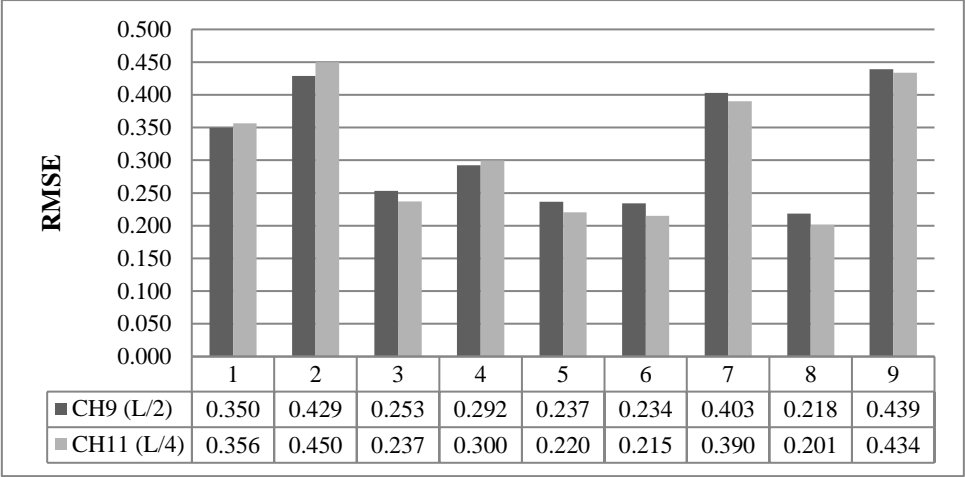


Figure21